Chemistry Europe
European Chemical Societies Publishing

WILEY VCH

Excellence in Chemistry Research

Announcing our new flagship journal

- Gold Open Access
- Publishing charges waived
- Preprints welcome
- Edited by active scientists

Meet the Editors of *ChemistryEurope*

Luisa De Cola
Università degli Studi di Milano Statale, Italy

Ive Hermans
University of Wisconsin-Madison, USA

Ken Tanaka
Tokyo Institute of Technology, Japan

ChemPubSoc Europe

DOI: 10.1002/cssc.201700635

CHEMSUSCHEM Full Papers

High-Efficiency Perovskite Solar Cell Based on Poly(3-Hexylthiophene): Influence of Molecular Weight and Mesoscopic Scaffold Layer

Narges Yaghoobi Nia, Fabio Matteocci, Lucio Cina, and Aldo Di Carlo*[a]

Here, we investigated the effect of the molecular weight (MW) of poly 3-hexylthiophene (P3HT) hole-transport material on the performance of perovskite solar cells (PSCs). We found that by increasing the MW the photovoltaic performances of the cells are enhanced leading to an improvement of the overall efficiency. P3HT-based PSCs with a MW of 124 kDa can achieve an overall average efficiency of 16.2%, double with respect to the ones with a MW of 44 kDa. Opposite to spiro-OMeTAD-based PSCs, the photovoltaic parameters of the P3HT-based devices are enhanced by increasing the mesoporous TiO_2 layer thickness from 250 to 500 nm. Moreover, for a titania scaffold layer thickness of 500 nm, the efficiency of P3HT-based PSCs with high MW is larger than the spiro-OMeTAD based PSCs with the same scaffold layer thickness. Recombination reactions of the devices were also investigated by voltage decay and electrochemical impedance spectroscopy. We found that the relationship between P3HT MW and cell performance is related to the reduction of charge recombination and to the increase of the P3HT light absorption by increasing the MW.

Introduction

Since the first reports on perovskite solar cells (PSCs),[1] rapid progress has been made in the last years[2] and the actual certified power conversion efficiencies (PCEs), 22.1%,[3] is larger than multicrystalline Si cell (21.3%[3]). More exciting, to obtain that efficiency, the thickness of the perovskite layer is only about 300 nm, whereas 300 000 nm of silicon is required for Si cells.[4] Similarly, perovskite solar modules demonstrated for the first time in 2014[5] have reached an efficiency of 13%.[6]

The ABX_3 perovskite absorber (usually A is CH_3NH_3, B is Pb, Sn, and X is Cl, Br, I), exhibits strong light-harvesting properties across the entire visible solar spectrum,[1,2] as well as good electron and hole-carrier mobility owing to their special crystalline phase and ambipolar character.[7]

Typically, the most efficient PSCs use thin layers of mesoporous TiO_2 (mp-TiO_2) and 2,2′,7,7′-tetrakis(*N*,*N*-di-*p*-ethoxyphenylamine)-9,9′-spirobifluorene (spiro-OMeTAD) as scaffold layer and hole-transport material (HTM), respectively. However, spiro-OMeTAD synthesis is still complex and not very efficient, leading to a quite high retail price for this compound.[8]

Among the different classes of materials studied for solar cells, conjugated polymers have garnered particular interest for the realization of low-cost, large-area products.[9] In recent years, an increasing effort has been devoted to studying thiophene-based polymers with attached alkyl side chains (C_nH_{2n+1}) in the 3-position of the thiophene rings. The interest toward these conjugated polymers is owed to their fusibility,[10] good solubility,[11] and processability. Moreover, structural, electronic, optical, and transport properties can be easily tuned by varying the length of the side chains,[12] temperature,[13] molecular weight (MW),[14] and applying directional crystallization techniques.[15] Compared to low-MW materials, polymers tend to be more disordered and to exhibit a hierarchical microstructure. Even chemically very regular and crystallizable, polymers usually form semicrystalline materials and display a crystalline/amorphous superstructure on a scale comparable to the size of the chain.[15] Poly(3-hexylthiophene) (P3HT) has the highest charge-carrier mobility among the conjugated polymers, showing hole mobility values as high as 0.1 $cm^2 V^{-1} s^{-1}$.[16] Moreover, P3HT has a band gap of 1.9–2.0 eV, which matches well with the maximum of the sunlight spectrum.[17] These merits make P3HT a good candidate for the absorbing blends in polymer photovoltaic cells.[18–20]

There are some investigations in the literature about the influence of P3HT MW on the charge-carrier mobility.[21–23] When increasing the MW, the charge carrier mobility increases and the absorption spectrum shows a red shift.[24] Goh et al. investigated the transport properties in the direction perpendicular to the substrate of region-regular P3HT with different MW in a diode geometry.[23] They showed that the mobility at room temperature increases from 1.333×10^{-5} to 3.303×10^{-4} $cm^2 V^{-1} s^{-1}$ as the MW increased from 2.9 to 31.1 kDa. Moreover, the mobility is found to be field independent for high MW films, but field dependent for the low MW films.

[a] *Dr. N. Y. Nia, Dr. F. Matteocci, Dr. L. Cina, Prof. A. Di Carlo*
Centre for Hybrid and Organic Solar Energy (CHOSE)
University of Rome Tor Vergata
Via del Politecnico 1, Rome 00133 (Italy)
E-mail: aldo.dicarlo@uniroma2.it

Supporting Information for this article can be found under: https://doi.org/10.1002/cssc.201700635.

This publication is part of dual Special Issues on "Perovskite Optoelectronics", published in *ChemSusChem* and *Energy Technology*. Please visit the *ChemSusChem* issue at **http://doi.org/10.1002/cssc.v10.19**, and the companion issue of *Energy Technology* at **http://dx.doi.org/10.1002/ente.v5.10**.

Some of these properties are related to the influence of the MW on the P3HT structure. Although the long period and presumably the crystal thickness (as observed by AFM and grazing-incidence small-angle scattering, GISAXS)[14] increases with MW, experiments also seem to indicate that the amount of order decreases with increasing MW.[17] AFM images of high MW P3HT show a small scale nodular structure as opposed to a lamellar structure.[14] Moreover, Bragg intensities in XRD experiments become weaker for higher MW.[14] Several possible explanations are proposed to solve the obvious discrepancies. Neher and co-workers suggested that the correlation between mobility and MW is related to a larger distortion of the backbone in the low MW materials.[25] Kline et al., on the other hand, attributed the higher mobility in high MW materials to a higher interconnectivity of the crystalline network.[21] They showed that in-plane π-stacking peak increases when the mobility increases for a constant MW. When the MW is changed, this correlation breaks down, confirming that in-plane π-stacking does not cause the mobility–MW relationship. Thus, they suggested that a combination of disordered domain boundaries and inherent effects of chain length on the electronic structure cause the mobility–MW relationship. This positive relationship between MW and mobility found for field-effect transistor (FET) mobility measurement was not confirmed by the bulk time-of-fly measurements of Ballantyne et al.[26] They showed that both hole and electron mobility in pristine P3HT films (as well as in PCBM:P3HT blends, PCBM = [6,6]-phenyl C_{61} butyric acid methyl ester) decrease as the MW is increased from 13 to 121 kDa owing most probably to a change in packing of the polymer chains. Thus, the relationship between MW and mobility in P3HT is still open to discussion and several theoretical investigations have been focused on this issue.[27]

The relationship between P3HT and MW in organic photovoltaic (OPV) and polymeric solar cells has been considered by several authors.[26,28–31] Although the effect of MW on the performance of P3HT has been emphasized in OPV device architectures, somewhat conflicting experimental results have been reported by different groups, and the reasons for the variations observed as a function of MW remain ambiguous. The variations in hole mobility with MW were found to correlate with substantial changes in thin-film morphology for blends with PCBM, leading to a subsequent drop in OPV device performance for MW > 34 kDa[26] Thus, it was postulated that higher MW fractions possess a higher degree of entanglement, hindering intrachain carrier transport by increasing the density of traps, while also impeding interchain hopping by diminishing the π-overlap between backbones. Careful investigation of the gelation mechanism, including fiber formation, of P3HT in *o*-xylene solutions has revealed a distinct two-step process involving π–π aggregation and thermos reversible gelation, in a MW-dependent mechanism in which individual aggregated chains link to each other.[28] OPV devices processed from *o*-xylene from various MW fractions of P3HT achieved a maximum PCE (~3.6%) for (weight average) MW = 43.7 and 72.8 kDa, but decreased at lower and higher MW. Ma et al. investigated the morphology and performance of bulk heterojunction solar cells comprised of P3HT and PCBM by varying P3HT MW.[29] They concluded that the optimum annealing temperature for the bulk heterojunction material is related to the MW of P3HT. The best performance was obtained by using P3HT with an optimum ratio between high MW and low MW components. The corresponding "ideal morphology" is comprised of highly ordered crystalline regions formed by low MWP3HT embedded and interconnected by a high MW P3HT matrix. One consistent trend among these studies is the observation of a clear effect of MW on the fibrillar morphology of P3HT, which affects carrier mobility and device performance.

Owing the good transport properties, P3HT has also been considered as HTM for PSCs[32] and the composition of P3HT with single-walled carbon nanotubes (SWNTs) and poly(methyl methacrylate) (PMMA) has shown good PSC stability.[33] However, despite the strong influence of MW of the structural and charge-transport properties of P3HT, there are no reports on the correlation between MW and P3HT-based PSCs performances. The purpose of this work is to shed light on this correlation. To this end, we used P3HTwith various MWs ranging from 44 to 124 kDa as HTM in PSCs. Current density–voltage (*J–V*) measurements of the solar cells were investigated under AM 1.5G irradiation and photovoltaic parameters like open-circuit voltage (V_{oc}), short-circuit current density (J_{sc}), fill factor (FF), and the overall efficiency were evaluated and compared to PSCs realized with spiro-OMeTAD. In addition, the influence of the scaffold layer thickness on the cell performance was evaluated by two mp-TiO_2 thicknesses, 250 and 500 nm. To further investigate MW effects on the electron recombination and electron lifetime, electrochemical impedance spectroscopy (EIS) and voltage decay measurements were evaluated.

Results and Discussion

Average photovoltaic parameters of P3HT-based PSCs with different MWs and two scaffold layer thicknesses (250 and 500 nm) are reported in Table 1 and Figure 1 together with the parameters for spiro-OMeTAD-based PSCs. Stabilized maximum power point (MPP) measurements are also reported in Figure S1 in the Supporting Information. Statistical distribution of measured cells is reported in Figures S2 and S3.

The PCE of the cells is enhanced by increasing the P3HT MW irrespectively of the mp-TiO_2 thicknesses. The relation between PCE and MW is mainly owed to the increase of J_{sc} and FF. On the other hand, V_{oc} does not present a direct correlation with the P3HT MW. Comparing the two HTMs, we observe that for P3HT-based PSCs, the increase of the mp-TiO_2 layer thickness results in an increase of J_{sc}, whereas the opposite if found for spiro-OMeTAD-based PSCs. Similar results were also found by Ding et al.,[34] who evaluated the impact of poly({4,8-bis[(2-ethylhexyl)oxy]benzo[1,2-b:4,5-b′]dithiophene-2,6-diyl}{3-fluoro-2-[(2-ethylhexyl)carbonyl]thieno[3,4-b]thiophenediyl}) (PTB7) MW on the organic photovoltaic performance showing an enhancement of J_{sc} and FF without any variation in V_{oc} by increasing the MW. They attributed these effects to the lower density of recombination centers and better photoactive layer morphology in the samples with higher MWs.

Table 1. Average values of photovoltaic parameters of spiro-OMeTAD and P3HT-based PSCs under AM 1.5G irradiation.

Sample	mp-TiO_2 thickness [nm]	V_{oc} [V]	J_{sc} [mA cm^{-2}]	FF	PCE [%]
P3HT-44 kDa	250	0.951 ± 0.019	10.74 ± 0.69	0.480 ± 0.019	4.92 ± 0.60
	500	0.942 ± 0.046	9.55 ± 1.28	0.530 ± 0.067	4.87 ± 1.44
P3HT-54 kDa	250	0.963 ± 0.018	13.42 ± 0.74	0.550 ± 0.019	7.12 ± 0.60
	500	1.011 ± 0.018	14.52 ± 2.66	0.528 ± 0.051	7.87 ± 2.14
P3HT-77 kDa	250	0.950 ± 0.018	13.71 ± 0.45	0.620 ± 0.016	8.07 ± 0.24
	500	1.017 ± 0.013	18.31 ± 1.80	0.629 ± 0.039	11.66 ± 0.62
P3HT-94 kDa	250	0.98 ± 0.012	13.80 ± 0.66	0.643 ± 0.015	8.69 ± 0.40
	500	1.031 ± 0.012	21.81 ± 0.24	0.659 ± 0.051	14.82 ± 1.05
P3HT-124 kDa	250	0.984 ± 0.012	15.55 ± 0.73	0.627 ± 0.011	9.59 ± 0.54
	500	1.024 ± 0.009	23.19 ± 1.20	0.686 ± 0.065	16.27 ± 1.48
spiro-OMeTAD	250	1.033 ± 0.022	21.87 ± 1.20	0.719 ± 0.012	16.24 ± 0.66
	500	1.046 ± 0.020	17.39 ± 0.70	0.692 ± 0.056	12.56 ± 0.81

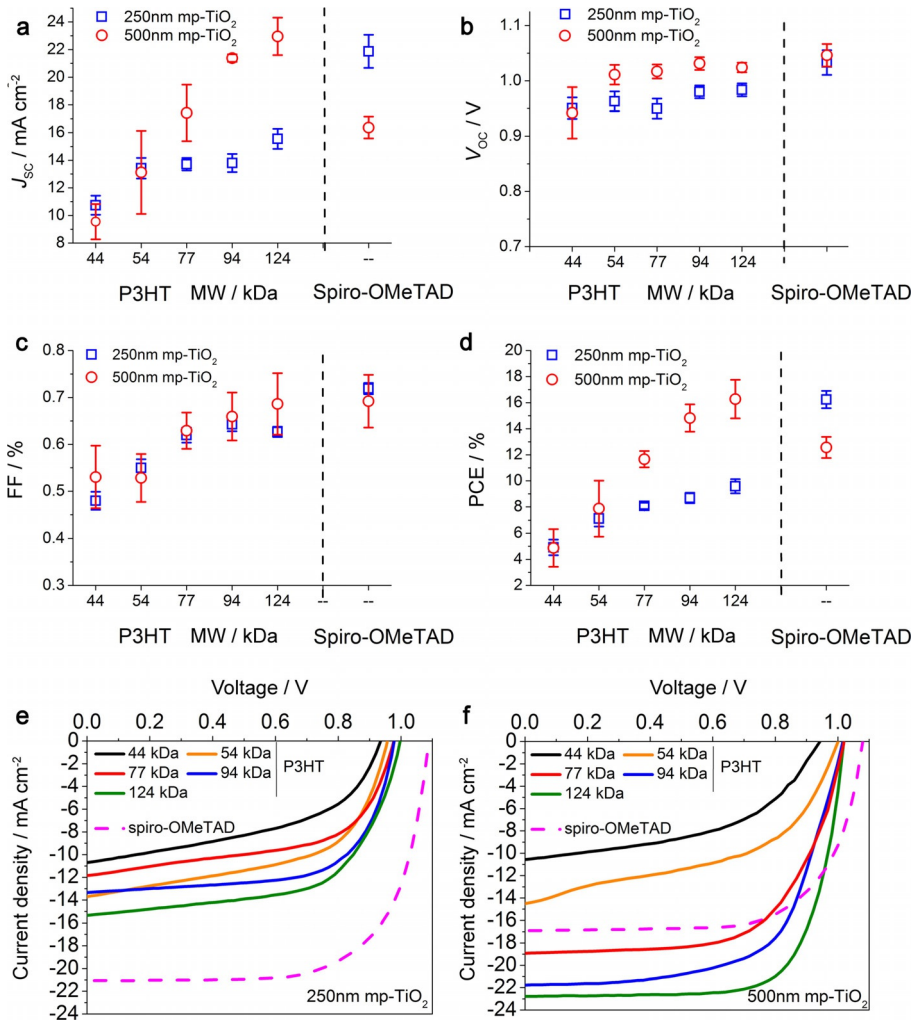

Figure 1. Statistics of photovoltaic parameters, a) J_{sc}, b) V_{oc}, c) FF, and d) PCE, for spiro-OMeTAD and for P3HT-based PSCs with different MWs. Two mp-TiO_2 thickness (250 and 500 nm) are also considered. *J–V* plots of typical PSCs with e) 250 nm, and f) 500 nm thickness of mp-TiO_2.

The observed MW dependence of the PCE of P3HT-based PSCs may be in part explained considering that by increasing the MW, domain boundaries and inherent enhancement of the chain length lead to better charge-carrier transport over a larger extent.[21,35,36] These effects will influence mainly the J_{sc} (Figure 1a) and the FF (Figure 1c), which will increase by increasing the MW, as has been also found in polymeric and TiO_2/P3HT hybrid solar cells.[37] Moreover, as will be discussed later, the light absorption of P3HT increases by increasing the MW leading to the PCE enhancement.

Capacitive characteristics of solar cells can affect the transient time to reach the steady-state condition and may lead to the *J–V* hysteresis as observed in PSCs.[38] Figure S4 shows *J–V* curves of typical spiro-OMeTAD and P3HT-based (different MWs) PSCs with same thickness of mp-TiO_2 (500 nm) obtained from the forward scan (FS, from short-circuit to open-circuit voltage bias) and reverse scan (RS, from open-circuit to short-circuit voltage bias). Photovoltaic parameters measured under FS and RS are also reported in the Supporting Information (Table S1). We do not observe a strong correlation between MW and the hysteresis phenomena even if the hysteresis for the higher MWs is quite negligible.

The relationship between FF and MW can be attributed to the electron-hole recombination, which reduces by increasing MW. The analysis of recombination phenomena was performed by combining dark *J–V*, open-circuit voltage decay (OCVD) and EIS measurements. For this analysis, only the set with 500 nm scaffold layer thickness was evaluated by comparing the different P3HT MWs with the reference spiro-OMeTAD. EIS plots and equivalent fitting circuit of the high MW P3HT-based device with 500 nm thickness of mp-TiO_2 are presented in Figure S5. The dark *J–V* plots in forward bias (Figure 2a) suggest lower recombination processes for higher P3HT MW. In particular, the 124 kDa sample shows the lowest recombination current for the entire voltage range. The dynamics associated to the recombination processes can be investigated by the OCVD test in which the full photovoltage decays from 1 sun to the state of dark equilibrium is recorded.[39,40] As the TiO_2 and perovskite layers are equal for all analyzed samples, the results obtained by OCVD allows to relate the free-charge recombination kinetics, expressed in terms of the decay time (Figure 2b), to the HTM layer composition.[41] As reported in Figure 2b, P3HT-based solar cells with higher MWs show higher decay times, which can be attributed to a slow-down of recombination processes by reducing the recombination path as well as enhancing charge extraction. This can explain the increase of the FF as a function of the MW.

The relationship between charge recombination and P3HT MW was elucidated by EIS analysis performed at different potentials under dark conditions. Complex spectra were fitted by a transmission-line-based model as reported recently[42] and presented in Figure S5.Constant phase elements (CPE) for chemical and HTM capacitances were used to achieve a good fit with experimental EIS data. The CPE ideality factor was taken into account for the extraction of the free-carrier lifetime. One of the key parameters is the distributed interfacial charge-transfer (recombination) resistance (R_{ct}) that takes into account the recombination of the free charges with the perovskite/HTM layer.[43,44] Higher R_{ct} indicates less recombination and, hence, higher free-charge lifetime and better charge collection that results on higher efficiency.[42,45] Interestingly, as showed in Figure 2c, R_{ct} is strongly affected by the MW of the P3HT. The R_{ct} increases more than two orders of magnitude, at intermediate voltage range, by varying the P3HT MW from 44 to 124 kDa. This confirms that the interfacial electron transfer with HTM can be influenced by the P3HT MW.[46] This result is also confirmed by the free-carrier effective lifetime (Figure 2d) obtained as the product between R_{ct} and the distributed chemical capacitance (C_u). Longest life times are obtained for 124 kDa MW reaching values greater than the reference cell under intermediate voltages.

The relation between J_{sc} and MW is also determined by the peculiar dependence of the external quantum efficiency (EQE) and light absorption on the P3HT MW. The EQE spectra (Figure 3a) for cells with 250 nm mp-TiO_2thickness show a broad peak in the range between 300 and 800 nm owing to the ab-

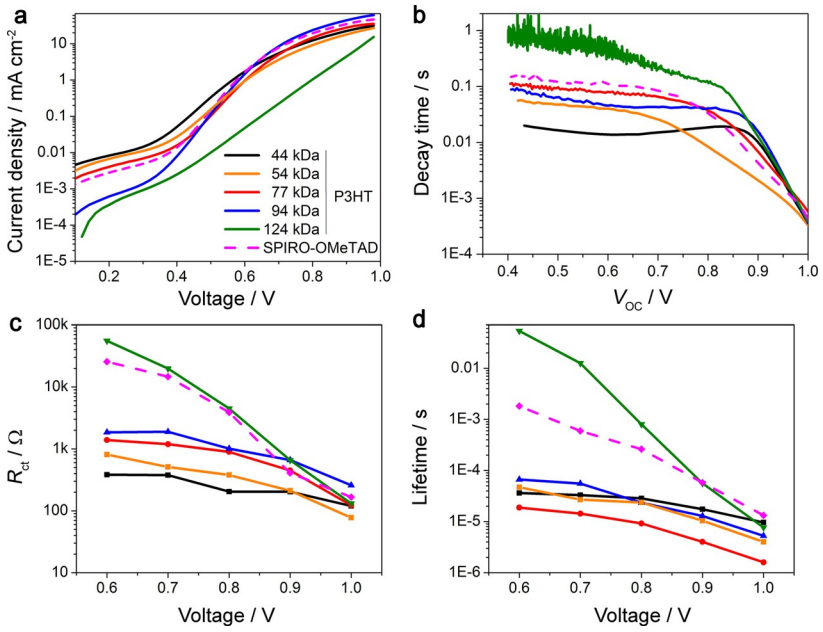

Figure 2. a) Dark *J–V* plots, b) decay time values extracted from OCVD analysis for PSCs made with several MWs of P3HT and with spiro-OMeTAD, c) recombination resistance/charge transfer interfacial resistance (R_{ct}) extracted from EIS under different bias potential in dark conditions, d) effective carrier lifetime calculated as the product between R_{ct} and the chemical capacitance (C_u).

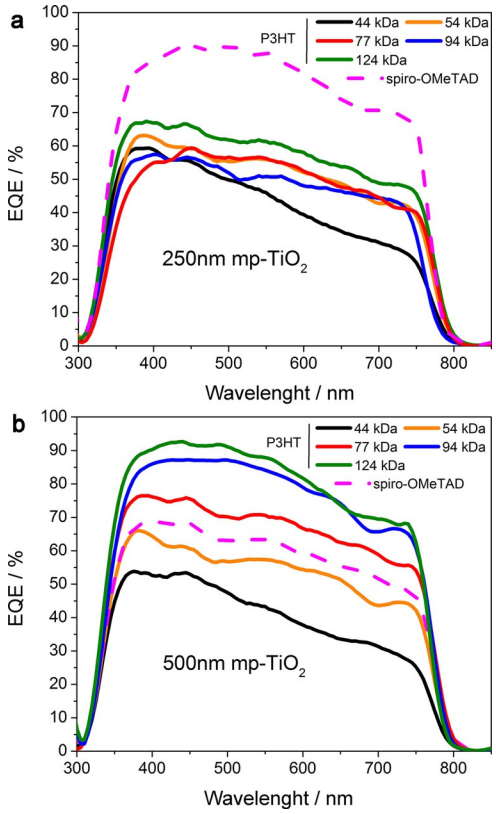

Figure 3. EQE spectra of selected spiro-OMeTAD and P3HT-based PSCs with a) 250 nm and b) 500 nm thickness of mp-TiO_2 layer.

sorbance of the perovskite layer. EQE values for these P3HT PSCs are enhanced by increasing the MW reaching a maximum value higher than 65% at 400 nm wavelength for the 124 kDa P3HT. This justifies the increase of the J_{sc} by increasing the P3HT MW shown in Figure 1b (J_{sc} extracted from EQE is presented in Figure S6). This is consistent with the J_{sc} plot of Figure 1b. Similarly, devices with mp-TiO_2 thicknesses of 500 nm present an EQE spectrum that is enhanced by increasing the P3HT MW up to a maximum above 90% at 450 nm wavelength. For such mp-TiO_2 thicknesses, the spiro-OMeTAD-based PSC shows a lower EQE with respect to the one with 250 nm mp-TiO_2, in agreement with Figure 1b.

To understand the relationship between the EQE and MW, we measured the absorbance spectra of the P3HT layers on glass having the same thickness as the one used in PSCs, namely 120 nm ± 20 nm (Figure 4). Generally, we observe that an increase of MW leads to an enhancement of the P3HT absorbance as was also reported by Peng et al.[47] for low-MW (4–10 kDa). This phenomenon could be explained by the increase of linear conformers[48] and chains alignment[49] by increasing the MW. Normalized absorbance of P3HT (Figure 4b) shows the typical behavior related to π–π* absorption transitions at ~607, ~558, and ~525 nm for all MWs.[36,50]

The absorbance peaks at 525 nm provides information on the degree of conjugation of the P3HT chains, whereas the peak at around 607 nm provides information on the degree of interchain order.[50] At low MW the intensity of the 607 nm peak is lower with respect to intermediate MW suggesting

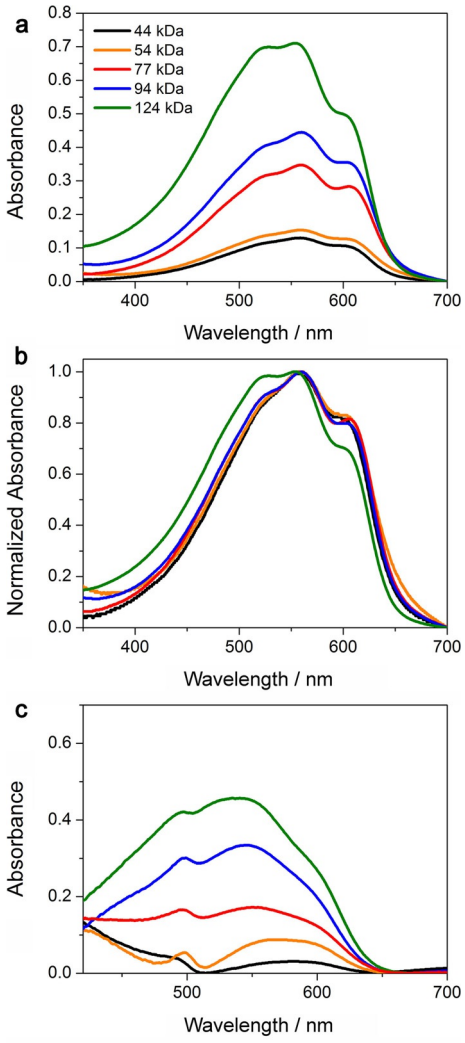

Figure 4. Absolute (a) and normalized (b) absorbance of P3HT deposited on glass (thickness = 120 nm ± 20 nm) for several MWs. c) Absorbance curves of P3HT-based perovskite solar cells (before Au coating) with 500 nm thickness of mp-TiO_2. Plots in (c) are obtained by subtracting the absorption of perovskite layer.

a short-conjugation length that increases by increasing the MW up to 54–77 kDa. A further MW increase reduces the intensity of this transition indicating a shortening of the conjugation length.[36]

To further confirm the strong impact of MW on P3HT absorbance also when this is used in the cell, we performed absorbance measurements of the complete P3HT-based PSC before Au coating. Results are shown in Figure 4c in which the absorption of the perovskite layer was subtracted (see Figure S7 for data with perovskite). The light absorbance of the cells increases by increasing the P3HT MW and a blue shift of the middle broad peak (from 540 to 580 nm) is found by varying the MW from 44 to 124 kDa. Upon crystallization, conductive polymers like P3HT generally form lamellar crystals separated by amorphous layers.[14] Polymer chains can fold in the amorphous parts to form more domain boundaries in the thin film layer.[25,51,52] This folding behavior is more evident for higher MWs that have longer chains and seems to be responsible for this blue shift.[25]

Conclusions

Here, we studied perovskite solar cells (PSCs) realized by using poly(3-hexylthiphene) (P3HT) hole-transport layer (HTL) focusing on the relation between P3HT molecular weight (MW) and the photovoltaic characteristics of the solar cells. Results clearly show a strong dependence of the cell efficiency on the P3HT MW: the larger the MW the higher the efficiency. The best efficiencies are achieved for MW of 124 kDa and for a thickness of mesoporous TiO_2 of 500 nm. Efficiency enhancement is mainly related to the increase of the short-circuit current (J_{sc}) and fill factor (FF) as P3HT MW increases.

The reason for this dependence can be attributed to two concomitant effects: an increase of the electron lifetime and the P3HT absorbance when the MW is increased. The increase of the lifetime is related to the increase of interfacial charge-transfer resistance, R_{ct}, that takes into account the recombination of the free charges with the perovskite/HTL. R_{ct} increases more than two orders of magnitude by varying the P3HT MW from 44 to 124 kDa. The increase of P3HT absorption for larger MW provides an additional contribution to the PSCs external quantum efficiency (EQE). The relation between MW and P3HT absorption has been found recently also for other polymers and it is related to the increase of linear conformers owing to the increased strength of chain–chain interactions.[48]

Experimental Section

A raster scanning laser (Nd:YVO_4 pulsed at 30 kHz average output power $P = 10$ W) was used to etch the fluorine-doped tin oxide (FTO) glass substrates (Pilkington, 8 $\Omega\,cm^{-1}$, 25 mm × 25 mm). The patterned substrates were cleaned in an ultrasonic bath, using detergent with deionized water, acetone, and 2-propanol (10 min for each step).A patterned compact TiO_2 (c-TiO_2) layer was deposited onto the patterned FTO by spray pyrolysis deposition using a previously reported procedure.[53] Briefly, the substrate temperature was fixed at 450 °C, the distance between the substrate positioned flat and the aerograph (tilted about 45° respect to the substrate) was fixed to 20 cm. The number of successive spray cycles was about 15 and the final thickness was 50 nm. Precursor spray solution was consisted of 0.16 M diisopropoxidytitanium bis(acetylacetonate) (TAA) and 0.4 M acetylacetone (ACAC) in ethanol. Patterning of the c-TiO_2 was achieved using a screen-printed metal mask that was removed after the c-TiO_2 deposition using an acidic solution, deionized water, and ethanol. A nanocrystalline mesoporous TiO_2 layer (18NR-Tpaste, Dyesol), diluted with ethanol, with *w*/*w* ratio of 1:4, was spin-coated onto the c-TiO_2 surface and sintered using the following annealing program: the temperature was increased from room temperature to 120 °C in 5 min, then the temperature was held for 5 min before increasing to 325 °C in 15 min; this temperature was maintained for 5 min and then increased to 375 °C, which was held for 5 min, and then increased to its final temperature of 480 °C in 5 min, which was kept constant for 30 min. To measure the final thickness of the mp-TiO_2 a Dektak-Veeco 150 profilometer was used.

The lead iodide solution (PbI_2 in *N*,*N*-dimethylformamide, 500 mg mL^{-1}, 1.08 M) was deposited by a spin-coating technique with 6000 rpm for 10 s with 6000 as an acceleration rate then dried at 70 °C for 10 min.

$CH_3NH_3PbI_3$ crystallization was achieved by dipping the PbI_2 layers in a methylammonium iodide solution (CH_3NH_3I in anhydrous 2-propanol, 10 mg mL^{-1}) for 10 min, washing immediately with 2-propanol by spin coating at 6000 rpm with 6000 as an acceleration rate for 10 s and dried at 100 °C for 10 min.

The two HTLs were deposited by spin-coating solution of 2,20,7,70-tetrakis-(*N*,*N*-dip-methoxyphenylamine)-9,9′-spirobifluorene (spiro-OMeTAD HTL, 73.2 mg mL^{-1}) or a solution of poly(3-hexylthiphene) (P3HT-HTL, 0.16 mM) with different MWs of 44, 54, 77, 94, and 124 kDa in chlorobenzene (the P3HT solutions were heated to 55 °C to prevent of any gel formation process)[28]. For P3HT HTLs, spin coating rpm was varied by varying the MW to achieve an equal thickness (130–140 nm) for all the HTM layers. Spiro-OMeTAD was deposited by spin-coating at 2000 rpm for 20 s and 2000 as acceleration rate. The spiro-OMeTAD and P3HT precursors were purchased from Sigma–Aldrich and Merck companies, respectively. Deposited P3HT was doped with of *tert*-butylpyridine (TBP, 11.4 μL) and of lithium bis(trifluoromethanesulfonyl)imide (LiTFSI, 12 μL) solution (520 mg in 1 mL of acetonitrile). Furthermore, spiro-OMeTAD was doped 7.2 μL of cobalt 209 (stock solution 375 mg in 1 mL acetonitrile) in further of same concentrations of TBP and LiTFSI. Conductivity of P3HT samples is dominated by doping and they were similar for all MWs (see Table S2).The thickness of all samples was measured with profilometer (DektakVeeco 150). Samples were introduced into a high-vacuum chamber (10^{-6} mbar) to thermally evaporate Au back contacts (thickness 80 nm). SEM and optical microscopic images from the surface of different layers are presented in Figure S8. In the present work, the deposition of perovskite and P3HTs layers were performed under atmospheric condition. For each P3HT MW as well as for spiro-OMeTAD PSCs batches of 8 cells were realized.

Masked devices were tested under a solar simulator (ABET Sun 2000, class A) at AM 1.5G and 100 mW cm^{-2} illumination conditions calibrated with a certified reference Si cell (RERA Solutions RR-1002). Incident power was measured with a Skye SKS 1110 sensor. PSC measurements were performed following the suggestion given in Refs. [54, 55]. Consistency check between J_{sc} as extracted by the *J*–*V* measurements and by EQE measurements are reported in Figures S6, S9, S10 and in Table S3.The absorbance was measured with a BLACK-Comet UV/Vis spectrometer. The morphology and grain size of the PbI_2, perovskite, and HTM layers were obtained by using SEM (FE-SEM ZEISS). EIS measurements were performed in dark conditions at room temperature using an Autolab 302N modular potentiostat from Metrohm in the two-electrode configuration with a bias voltage ranging from 0.6 to 1 V. The sinewave ac perturbation was used 10 mV of amplitude with frequencies from 1 MHz to 1 Hz. OCVD measurements were performed with a white LED-based measurement system (Arkeo—Cicci research srl).

Acknowledgements

The research leading to these results has received funding from the European Union Seventh Framework Program (FP7/2007-2013) under Grant Agreement 316494 (DESTINY) and Grant Agreement n. 609788 (CHEETAH). The authors gratefully acknowledge the project PERSEO-"PERrovskite-based Solar cells: towards high Efficiency and long-term stability" (Bando PRIN 2015-Italian Ministry of University and Scientific Research (MIUR) Decreto Direttoriale 4 novembre 2015 n. 2488, project number 20155LECAJ)

for funding. Authors gratefully acknowledge Dr. Luigi Salamandra for his useful information about polymer optimization.

Conflict of interest

The authors declare no conflict of interest.

Keywords: halides · hole-transport material · molecular weight · poly(3-hexylthiophene) · perovskite solar cells

[1] A. Kojima, K. Teshima, Y. Shirai, T. Miyasaka, *J. Am. Chem. Soc.* **2009**, *131*, 6050; H.-S. Kim, C.-R. Lee, J.-H. Im, K.-B. Lee, T. Moehl, A. Marchioro, S.-J. Moon, R. Humphry-Baker, J.-H. Yum, J. E. Moser, M. Grätzel, N.-G. Park, *Sci. Rep.* **2012**, *2*, 591; M. M. Lee, J. Teuscher, T. Miyasaka, T. N. Murakami, H. J. Snaith, *Science* **2012**, *338*, 643.

[2] N. J. Jeon, J. H. Noh, W. S. Yang, Y. C. Kim, S. Ryu, J. Seo, S. I. Seok, *Nature* **2015**, *517*, 476.

[3] National Renewable Energy Laboratory (NREL) Efficiency Chart, http://www.nrel.gov/ncpv/images/efficiency_chart.jpg (accessed on 4th March 2017).

[4] T. Saga, *NPG Asia Mater.* **2010**, *2*, 96.

[5] F. Matteocci, S. Razza, F. Di Giacomo, S. Casaluci, G. Mincuzzi, T. M. Brown, A. D'Epifanio, S. Licoccia, A. Di Carlo, *Phys. Chem. Chem. Phys.* **2014**, *16*, 3918.

[6] F. Matteocci, L. Cinà, F. Di Giacomo, S. Razza, A. L. Palma, A. Guidobaldi, A. D'Epifanio, S. Licoccia, T. M. Brown, A. Reale, A. Di Carlo, *Prog. Photovolt: Res. Appl.* **2016**, *24*, 436.

[7] E. Edri, S. Kirmayer, A. Henning, S. Mukhopadhyay, K. Gartsman, Y. Rosenwaks, G. Hodes, D. Cahen, *Nano Lett.* **2014**, *14*, 1000.

[8] N. J. Jeon, H. G. Lee, Y. C. Kim, J. Seo, J. H. Noh, J. Lee, S. I. Seok, *J. Am. Chem. Soc.* **2014**, *136*, 7837.

[9] J. H. Heo, S. H. Im, J. H. Noh, T. N. Mandal, C.-S. Lim, J. A. Chang, Y. H. Lee, H.-J. Kim, A. Sarkar, K. Nazeeruddin, M. Grätzel, S. I. Seok, *Nat. Photonics* **2013**, *7*, 486.

[10] H. Yang, T. J. Shine, L. Yang, K. Cho, C. Y. Ryu, Z. Bao, *Adv. Funct. Mater.* **2005**, *15*, 671.

[11] M. J. Winokur, D. Spiegel, Y. Kim, S. Hotta, A. J. Heeger, *Synth. Met.* **1989**, *28*, 419.

[12] A. Gadisa, W. D. Oosterbaan, K. Vandewal, J.-C. Bolsée, S. Bertho, J. D'Haen, L. Lutsen, D. Vanderzande, J. V. Manca, *Adv. Funct. Mater.* **2009**, *19*, 3300.

[13] S. Tiwari, W. Takashima, S. K. Balasubramanian, S. Miyajima, S. Nagamatsu, S. S. Pandey, R. Prakash, *Jpn. J. Appl. Phys.* **2014**, *53*, 021601.

[14] Z. Wu, A. Petzold, T. Henze, T. Thurn-Albrecht, R. H. Lohwasser, M. Sommer, M. Thelakka, *Macromolecules* **2010**, *43*, 4646.

[15] R. Colle, G. Grosso, A. Ronzani, C. M. Zicovich-Wilson, *Phys. Status Solidi B* **2011**, *248*, 1360.

[16] H. Sirringhaus, N. Tessler, R. H. Friend, *Science* **1998**, *280*, 1741.

[17] V. Shrotriya, J. Ouyang, R. J. Tseng, G. Li, Y. Yang, *Chem. Phys. Lett.* **2005**, *411*, 138.

[18] N. Camaioni, G. Ridolfi, G. C. Miceli, G. Possamai, M. Maggini, *Adv. Mater.* **2002**, *14*, 1735.

[19] F. Padinger, R. S. Rittberger, N. S. Sariciftci, *Adv. Funct. Mater.* **2003**, *13*, 85.

[20] I. Riedel, V. Dyakonov, *Phys. Status Solidi A* **2004**, *201*, 1332.

[21] R. J. Kline, M. D. McGehee, E. N. Kadnikova, J. Liu, J. M. J. Fréchet, M. F. Toney, *Macromolecules* **2005**, *38*, 3312.

[22] M. Brinkmann, P. Rannou, *Adv. Funct. Mater.* **2007**, *17*, 101.

[23] C. Goh, R. J. Kline, M. D. McGehee, E. N. Kadnikova, J. M. Fréchet, *J. Appl. Phys. Lett.* **2005**, *86*, 122110.

[24] R. Zhang, R. D. McCullough, *J. Am. Chem. Soc.* **2006**, *128*, 3480.

[25] A. Zen, J. Pflaum, S. Hirschmann, W. Zhuang, F. Jaiser, U. Asawapirom, J. Rabe, U. Scherf, D. Neher, *Adv. Funct. Mater.* **2004**, *14*, 757.

[26] A. M. Ballantyne, L. Chen, J. Dane, T. Hammant, F. M. Braun, M. Heeney, W. Duffy, L. McCulloch, D. D. C. Bradley, J. Nelson, *Adv. Funct. Mater.* **2008**, *18*, 2373.

[27] C. Poelking, K. Daoulas, A. Troisi, D. Andrienko, *Adv. Polymer* **2014**, *265*, 139.

[28] M. Koppe, C. J. Brabec, S. Heiml, A. Schausberger, W. Duffy, M. Heeney, I. McCulloch, *Macromolecules* **2009**, *42*, 4661.

[29] W. Ma, J. Y. Kim, K. Lee, A. J. Heeger, *Macromol. Rapid Commun.* **2007**, *28*, 1776.

[30] P. Schilinsky, U. Asawapirom, U. Scherf, M. Biele, C. J. Brabec, *Chem. Mater.* **2005**, *17*, 2175.

[31] P. M. Beaujuge, J. M. J. Frechet, *J. Am. Chem. Soc.* **2011**, *133*, 20009.

[32] F. Di Giacomo, S. Razza, F. Matteocci, A. D'Epifanio, S. Licoccia, T. M. Brown, A. Di Carlo, *J. Power Sources* **2014**, *251*, 152.

[33] I. K. Dind, N. Tetreault, J. Brillet, B. E. Hardin, E. H. Smith, S. J. Rosenthal, F. Sauvage, M. Grätzel, M. D. McGehee, *Adv. Funct. Mater.* **2009**, *19*, 2431.

[34] Z. Ding, J. Kettle, M. Horie, S. W. Chang, G. C. Smith, A. I. Shames, E. A. Katz, *J. Mater. Chem. A* **2016**, *4*, 7274.

[35] R. J. Kline, M. D. McGehee, E. N. Kadnikova, J. Liu, J. M. J. Fréchet, *Adv. Mater.* **2003**, *15*, 1519.

[36] J.-F. Chang, J. Clark, N. Zhao, H. Sirringhaus, D. W. Breiby, J. W. Andreasen, M. M. Nielsen, M. Giles, M. Heeney, I. McCulloch, *Phys. Rev. B* **2006**, *74*, 115318.

[37] M.-C. Wu, C.-H. Chang, H.-H. Lo, Y.-S. Lin, Y.-Y. Lin, W.-C. Yen, W.-F. Su, Y.-F. Chen, C.-W. Chen, *J. Mater. Chem.* **2008**, *18*, 4097.

[38] H.-S. Kim, N.-G. Park, *J. Phys. Chem. Lett.* **2014**, *5*, 2927.

[39] D. Bi, L. Yang, G. Boschloo, A. Hagfeldt, E. M. J. Johansson, *J. Phys. Chem. Lett.* **2013**, *4*, 1532.

[40] V. Roiati, S. Colella, G. Lerario, L. De Marco, A. Rizzo, A. Listorti, G. Gigli, *Energy Environ. Sci.* **2014**, *7*, 1889.

[41] L. Bertoluzzi, R. S. Sanchez, L. Liu, J.-W. Lee, E. Mas-Marza, H. Han, N.-G. Park, I. Mora-Sero, J. Bisquert, *Energy Environ. Sci.* **2015**, *8*, 910.

[42] A. Dualeh, T. Moehl, N. Tetreault, J. Teuscher, P. Gao, M. K. Nazeeruddin, M. Grätzel, *ACS Nano* **2014**, *8*, 362.

[43] J. M. Marin-Beloqui, L. Lanzetta, E. Palomares, *Chem. Mater.* **2016**, *28*, 207.

[44] Y. Wang, H.-Y. Wang, M. Yu, L.-M. Fu, Y. Qin, J.-P. Zhang, X.-C. Ai, *Phys. Chem. Chem. Phys.* **2015**, *17*, 29501.

[45] E. Guillén, F. J. Ramos, J. A. Anta, S. Ahmad, *J. Phys. Chem. C* **2014**, *118*, 22913.

[46] M. Cai, V. T. Tiong, T. Hreid, J. Bell, H. Wang, *J. Mater. Chem. A* **2015**, *3*, 2784.

[47] Q. Peng, I. W. Wyman, D. Han, G. Liu, *Can. J. Chem.* **2011**, *89*, 27.

[48] M. S. Vezie, S. Few, I. Meager, G. Pieridou, B. Dörling, R. S. Ashraf, A. R. Goñi, H. Bronstein, I. McCulloch, S. C. Hayes, M. Campoy-Quiles, J. Nelson, *Nat. Mater.* **2016**, *15*, 746.

[49] K. Koynov, A. Bahtiar, T. Ahn, R. M. Cordeiro, H. H. Hörhold, C. Bubeck, *Macromolecules* **2006**, *39*, 8692; A. Bahtiar, K. Koynov, T. Ahn, C. Bubeck, *J. Phys. Chem. B* **2008**, *112*, 3605.

[50] P. J. Brown, D. S. Thomas, A. Kohler, J. S. Wilson, J. S. Kim, C. M. Ramsdale, H. Sirringhaus, R. H. Friend, *Phys. Rev. B* **2003**, *67*, 064203; B. F. Xue, B. Vaughan, C. H. Poh, K. B. Burke, L. Thomsen, A. Stapleton, X. J. Zhou, G. W. Bryant, W. Belcher, P. C. Dastoor, *J. Phys. Chem. C* **2010**, *114*, 15797; T. S. Ripolles, A. Guerrero, G. Garcia-Belmonte, *Appl. Phys. Lett.* **2013**, *103*, 243306.

[51] H. Sirringhaus, P. J. Brown, R. H. Friend, M. M. Nielsen, K. Bechgaard, B. M. W. Langeveld-Voss, A. J. H. Spiering, R. A. J. Janssen, E. W. Meijer, P. Herwig, D. M. de Leeuw, *Nature* **1999**, *401*, 685.

[52] H. Wang, Y. Xu, X. Yu, R. Xing, J. Liu, Y. Han, *Polymer* **2013**, *5*, 1272.

[53] F. Matteocci, G. Mincuzzi, F. Giordano, A. Capasso, E. Artuso, C. Barolo, G. Viscardi, T. M. Brown, A. Reale, A. Di Carlo, *Org. Electron.* **2013**, *14*, 1882.

[54] E. Zimmermann, P. Ehrenreich, T. Pfadler, J. A. Dorman, J. Weickert, L. Schmidt-Mende, *Nat. Photonics* **2014**, *8*, 669.

[55] J. A. Christians, J. S. Manser, P. V. Kamat, *J. Phys. Chem. Lett.* **2015**, *6*, 852.

[56] B. K. Kuila, A. K. Nandi, *Macromolecules* **2004**, *37*, 8577.

Manuscript received: April 13, 2017
Revised manuscript received: May 21, 2017
Accepted manuscript online: May 29, 2017
Version of record online: June 14, 2017